RSC Advances

PAPER

View Article Online
View Journal | View Issue

Cite this: *RSC Adv.*, 2019, **9**, 3050

Synthesis, crystal structure, self-assembly of C_{60} derivatives bearing rigid pyridine substituents†

Min Ai,[a] Jie Li,[a] Zijuan Ji,[a] Chuanhui Wang,[a] Rui Li,[a] Wei Dai*[a] and Muqing Chen *[ab]

Received 1st December 2018
Accepted 12th January 2019

DOI: 10.1039/c8ra09893j

rsc.li/rsc-advances

Microstructures of fullerene derivatives formed *via* self-assembly strategy facilitate the versatile applications of these zero-dimensional molecules. However, the accurate elucidation of formation mechanism of fullerene microstructures is a challenge issue. A novel fullerene derivative **2** with rigid pyridine substituent was synthesized and characterized by X-ray crystallography. Using the strategy of liquid–liquid interfacial precipitation, self-assembly of **2** affords a micrometer-sized flowerlike and a discoid morphology. Based on the crystal packing of **2**, the proper formation mechanism of different morphologies was proposed. Meanwhile, the photoelectrochemical properties of different morphologies of **2** was also unveiled.

Introduction

Fullerene derivatives have attracted widespread interest in the fields of organic electronics, energy conversion and biomedicines due to their unique structures and physico-chemical properties.[1–4] As a zero-dimensional carbon molecule, fullerene has been regarded as a superior building block to construct versatile micro-/nano-structures with well-defined and controlled dimensionality.[5–7] Due to its high abundance among the family of fullerenes, C_{60} is widely functionalized toward constructing various nano/micro-structures with well-ordered one-dimensional (1D) or two-dimensional (2D) architectures by one-step liquid–liquid interfacial precipitation (LLIP) strategies,[8–10] template assisted dip drying[11] and drop-drying processes.[12,13] As far as we know, fullerene derivatives bearing versatile functional groups have been reported to self-assemble into versatile architectures such as spheres,[14] rods,[15] wires,[16] discs,[17] vesicles[18] and flowerlike objects.[19] Importantly, the substituents on the fullerene cage not only change the molecular solubility, but also affect the intermolecular assembly by steric hindrance and molecular polarity.

Moreover, the introduced substitutes onto fullerene cage play a vital role in self-assembly process because they provide a weak intermolecular force such as van der Waals forces, in addition to conventional strong π–π interactions between carbon cages.[20–26] To the best of our knowledge, among fullerene derivatives used for self-assembly, the attached substitutes mainly focus on long alkyl-chains or short aromatic moiety.[23,26–28] In contrast, long alkyl chains on fullerene cage facilitating to improve the solubility of fullerene derivatives, have a side-effect of reducing electronic activity of fullerene. The short aromatic moiety containing pyridine groups,[23] benzoate[28] and azo chromophore,[29] although results in the lower solubility in organic solvents, still enables fullerene derivatives to retain most electronic activity of fullerenes. Therefore, whether a fullerene derivative simultaneously possessing high electronic activity and solubility is desired for further self-assembly.

Herein, we synthesized a novel fullerene derivative **2** *via* a simple two-step reaction, in which a rigid and π-conjugated pyridine substituent composed of two phenyl rings and a marginal pyridine was attached onto fullerene cage, exhibiting good solubility in organic solvents such as toluene, chloroform, tetrahydrofuran. Molecular structure and electron properties of **2** were characterized by the combination measurements of NMR, MALDI-TOF, UV-vis spectra, electrochemistry and theoretical calculation. More importantly, single crystal of **2** was successfully obtained and corresponding molecular structure and crystal packing has been unambiguously confirmed by X-ray crystallography. The self-assembled morphologies of **2** were obtained by LLIP method. The formation mechanism of different morphologies was discussed in detail by combining with the crystal packing of **2**. Thereafter, the affection of these morphologies on photoelectrochemical properties was also investigated.

Results and discussion

Synthesis route of the novel fullerene derivative **2** was shown in Scheme 1 and detailed procedure is described in the experimental section. The molecular structure was analyzed by means of NMR (^{1}H, ^{13}C) and Matrix-Assisted Laser Desorption/Ionization Time of Flight Mass Spectrometry (MALDI-TOF MS)

[a]*School of Physics and Mechanical & Electronical Engineering, Hubei University of Education, 129 Gaoxin Second Road, Wuhan Hi-Tech Zone, Wuhan 430205, China. E-mail: daiwei@hue.edu.cn*

[b]*Department of Materials Science and Engineering, University of Science and Technology of China, Hefei 230026, China. E-mail: mqchen@ustc.edu.cn*

† Electronic supplementary information (ESI) available. CCDC 1578717. For ESI and crystallographic data in CIF or other electronic format see DOI: 10.1039/c8ra09893j

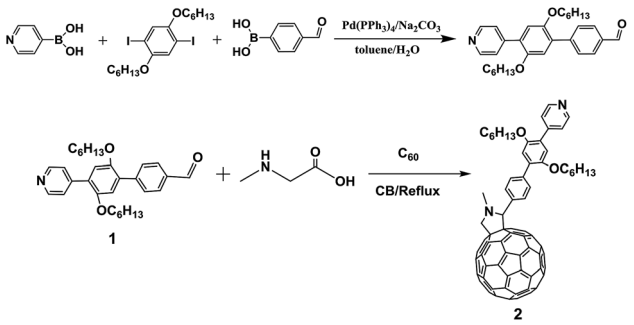

Scheme 1 Synthesis route of fullerene derivative **2**.

(Fig. S1†). More importantly, molecular structure and crystal packing of **2** was unambiguously confirmed by single-crystal X-ray diffraction (XRD) crystallography (Fig. 1). Black crystals suitable for crystal measurements were obtained by slow diffusion of *n*-hexane into carbon disulfide solution of **2** over a period of four weeks at room temperature. Although carbon disulfide and *n*-hexane were used to grow crystals, there is no evidence of solvent molecules in the crystals. Crystal structure of **2** shows that the cycloaddition reaction occurs at a [6,6]-bond with a closed-ring pattern. The bond length (C2A–C1A, 1.667(11) Å) between the two cage carbon atoms which involve the addition reaction, falls into the range of a C–C single bond, confirming the closed-ring structure of **2**. Additionally, the bond lengths of C2A–C61A, C1A–C63A, C63A–N1A and C61A–N1A are 1.56(2), 1.507(15), 1.450(8) and 1.561(13), respectively. The twisted five-membered pyrrole ring (C1A–C2A–C61A–N1A–C63A) attached onto carbon cage shows that nitrogen atom slightly deviates 48.28° from the plane comprised of four carbon atoms (C1A, C2A, C61A and C63A). The crystal packing of **2** exhibits a parallel and ordered distribution of fullerene region and rigid pyridine substituent shown in Fig. S2.†

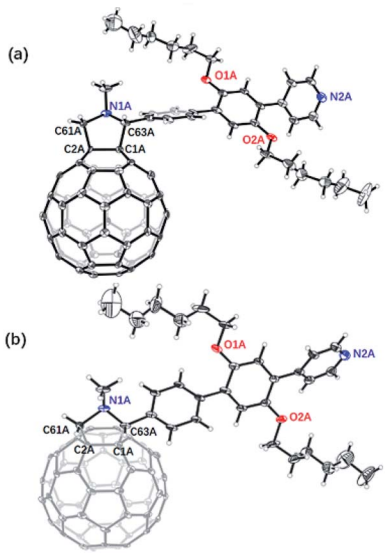

Fig. 1 Ortep drawing of **2** showing thermal ellipsoids at the 30% probability level. (a) Viewing from front side, (b) viewing from top side.

The electronic structure of **2** was investigated by UV-vis spectrography as illustrated in Fig. 2. Absorption spectrum of **2** resembles that of pristine C_{60}, showing similar characteristic peaks from UV to visible region. Specially, the enhanced absorption intensity of **2** in the region of 280–535 nm comparing to that of C_{60} was speculated to the interaction between C_{60} and rigid pyridine moiety.[17] Meanwhile, the characteristic peak of **2** at 433 nm indicates [6,6]-close addition pattern, which is consistent with results discussed in single crystal (Fig. 1a).

Cyclic voltammetry (CV) measurements were carried out to obtain redox properties of **2** at a scan rate of 100 mV s^{-1} in *o*-dichlorobenzene solutions using 0.1 M of *n*-Bu_4NPF_6 as supporting electrolyte (Fig. 3). CV curve of **2** exhibits three reversible redox peaks, while the first reduction peak shifts by 0.16 V to cathode under the same experimental conditions compared with that of C_{60}. The corresponding LUMO energy level of **2** calculated from onset for reduction potential is −3.76 eV by the following equation: LUMO = $-(E_{red} + 4.80)$ eV compared to that the LUMO energy level of C_{60} is −3.89 eV, demonstrating the higher stability of **2** than that of C_{60}. Theoretical calculation here is used to understand the electron structure of **2**, affording the corresponding energy level including HOMO (−5.47 eV) and LUMO (−3.5 eV), respectively, shown in Fig. 4. Meanwhile, no charge transfer from pyridine moiety to fullerene cage was observed under excitation.

The self-assembly of fullerene derivative **2** was further investigated by LLIP method. The experimental procedures are as followed. Toluene herein was employed as good solvent to dissolve **2** and hexane is as poor solvent. The concentration of **2** in toluene was set to be 10 mg mL^{-1}. 2 mL toluene solution of **2** was rapidly injected into 8 mL and 20 mL hexane, respectively, to instantly form turbid solution, leading to the formation of different microstructures. Then the two solutions were placed without moving for 12 h. The suspension was separated by centrifugation and then the precipitate was washed with hexane several times. Later, the samples were further treated by vacuum drying at 60 °C overnight to remove the solvents absorbed on surface of microstructures. Then, the two samples were characterized by scanning electron microscopy (SEM), showing different morphologies that one is flowerlike *versus* that another is discoid (Fig. 5b and d). The size distribution of flowerlike and

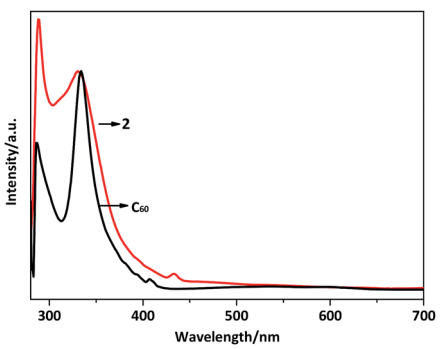

Fig. 2 UV-vis spectra of C_{60} and **2** in toluene.

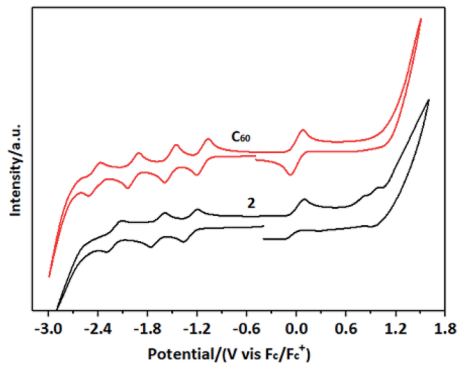

Fig. 3 CV profiles of **2** and C_{60}. Conditions: working electrode, Pt disc; counter electrode, Pt wire; reference electrode, Ag wire; supporting electrolyte, 0.1 M n-Bu_4NPF_6 in 1,2-dichlorobenzene; scan rate, 100 mV s^{-1}.

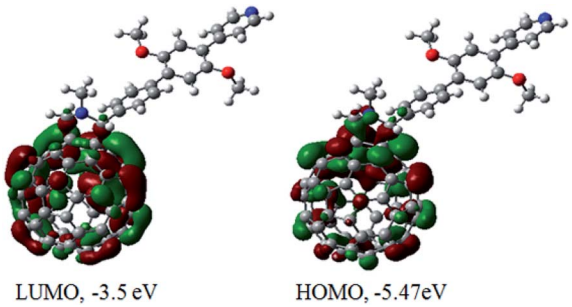

Fig. 4 The electronic distribution and energy level of **2** based on B3LYP/6-31g method. The hexyl was simplified as methyl for facilitating calculation.

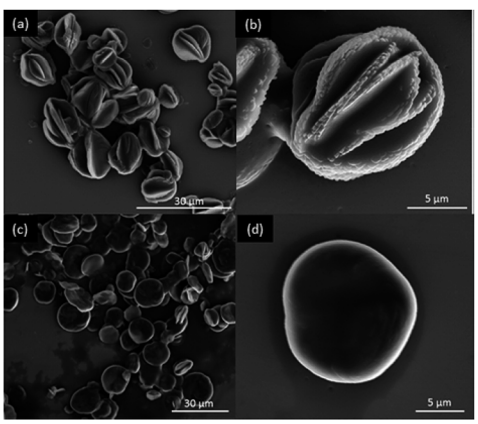

Fig. 5 SEM images of two different morphologies of **2**. The scale bars of insets in (a and c) and (b and d) are 30 μm and 5 μm, respectively.

discoid microstructures are 3–12 μm (Fig. 5a) and 2–13 μm (Fig. 5c), respectively.

The process of morphology growth is described in Scheme 2 similar with reported results.[28] First, the initial molecular arrangement for **2** leads to the formation of intermolecular dimer structure with antiparallel manner,[20] and further constructs the ordered subunits. Later, growth of molecular

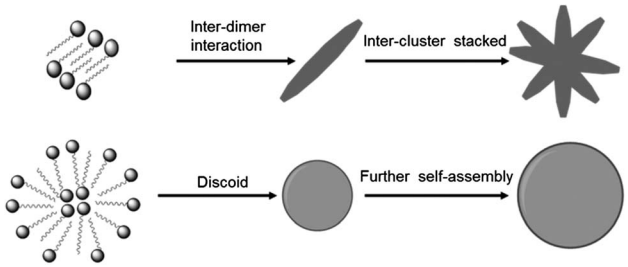

Scheme 2 Schematic of the formation mechanism of microstructures of **2** *via* LLIP method. The functional group in **2** is simplified as wavy line for clarity.

subunits by maximizing the most favored orientation leads to the formation of monopod or nano-discoid. These intermediate structures along a packing orientation lead to the final flower-like or discoid microstructures upon complete solvent diffusion.

Crystal packing of **2** was used to understand above mechanism proposed for self-assembly shown in Fig. 6. The molecules are self-assembled laterally to form the resultant structure, in which the rigid conjugated pyridine moiety is arranged in an antiparallel fashion perfectly consistent with initial formed dimers for flowerlike morphology in Scheme 2. Two pairs of intermolecular dimers in Fig. 6b show an obviously stacking tendency that fullerene cage region and pyridine moiety region is separated. The shortest distances for fullerene–fullerene and fullerene–pyridine moiety are 3.036 Å and 3.448 Å, respectively, compared to that of pyridine moiety–pyridine moiety (2.999 Å), exhibiting that strong interactions for cage–cage and pyridine moiety–pyridine moiety play an important role in self-assembly in addition to the solvent effect.

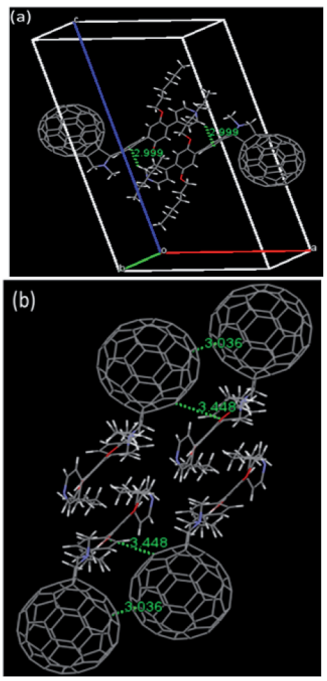

Fig. 6 (a) Crystal packing of **2** with a view from b axis, and (b) two pairs of dimers visualized through the a axis.

The photoelectrochemical properties for **2** with flowerlike (a) and discoid (b) microstructures are investigated and corresponding photoelectrochemical cells were fabricated according to the reported method.[30,31] The typical photocurrent response curves responding to each on–off event in the visible regions at a bias voltage of 1.0 V were shown in Fig. 7. The photocurrent response of a and b show anodic photocurrents response to each on–off event under positive bias voltage, indicating an n-type photo-response processes.[31] Specially, the photocurrent response of flowerlike microstructure (b) has 1.5 times higher than that of discoid microstructure (a), indicating that flowerlike microstructure may facilitate efficient charge carrier transport among them and decrease corresponding charge recombination losses.[31,32]

Experimental

Materials and methods

Scanning electron microscopy (SEM) images were collected using either a Nova NanoSEM 450 or a JEOL 6701F electron microscope operating at an accelerating voltage of 10 kV. UV-vis spectra were obtained using a Lambda 750S spectrometer. Matrix-assisted laser desorption-ionization time-of flight (MALDI-TOF) mass spectra were recorded with a Biflex III (Bruker Daltonics Inc., Germany) mass spectrometer using 1,1,4,4-tetraphenyl-1,3-butadiene as matrix in a positive ion linear mode. Cyclic voltammogram (CV) and differential pulse voltammogram (DPV) were measured in 1,2-dichlorobenzene (*o*-DCB) with 0.1 M of $(n\text{-Bu})_4NPF_6$ as supporting electrolyte at a Pt working electrode with a CHI660E workstation.

Photocurrent measurements. The photocurrent tests were carried out in a three-electrode system, consisting of a working electrode fabricated using two microstructure a and b, an Ag/AgCl reference electrode and a platinum wire counter electrode with a CHI660E electrochemical workstation at room temperature and a 500 W xenon lamp (Saifan Photoelectronic Co., 7IPX5002) as a light source. The electrolyte is 0.1 M aqueous KCl solution. The working electrode was made as follows: indium tin oxide (ITO) was used as the current collector and isopropanol dispersions of the corresponding two microstructures were deposited onto the ITO by drop-casting. The filter for photoelectrochemical cell was used to obtain the visible light source (400–800 nm). All photoelectrochemical experiments were carried out under Ar atmosphere.

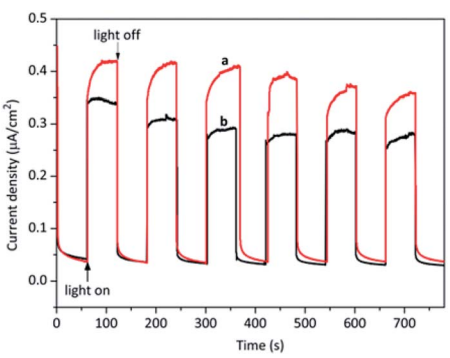

Fig. 7 Photocurrent response of **2** with flowerlike morphology (a) or discoid morphology (b). The arrows mark the light on–off cycles (1.0 V bias voltage, 0.1 M KCl electrolyte solution, 500 W white light illuminations).

Synthetic procedures

Synthesis of 1. Tetrahydrofuran (35 mL) was added to a mixture of 1,4-bis(hexyloxy)-2,5-diiodobenzene (3.2 g, 6.04 mmol), pyridine-4-boronic acid (0.62 g, 5.06 mmol), 4-formylphenylboronic acid (0.76 g, 5.06 mmol), sodium carbonate (4.15 g, 30 mmol) in a 100 mL flask with three necks under argon atmosphere. The solution was purged about 20 min by argon. Later, a solution of $Pd(PPh_3)_4$ (0.035 g, 0.03 mmol) in 5 mL of toluene was added into above mixture. Then the mixture was stirred and heated for 36 h at 120 °C. After the reaction, the mixture was washed with water and ethyl acetate. The organic layer was separated and dried over magnesium sulfate, filtrated, and concentrated for the purification by flash column chromatography (eluent, ethyl acetate/CS_2 = 1/9(v/v)), affording 0.65 g (31%) product **1**. ^{1}H NMR (600 MHz, acetone-d_6) δ 10.12 (s, 1H), 8.64 (d, J = 5.9 Hz, 2H), 8.01 (d, J = 8.2 Hz, 2H), 7.90 (d, J = 8.2 Hz, 2H), 7.70–7.63 (m, 2H), 7.23 (d, J = 5.3 Hz, 2H), 4.10 (q, J = 6.5 Hz, 4H), 1.77–1.70 (m, 4H), 1.46–1.38 (m, 4H), 1.30 (ddd, J = 10.2, 7.1, 3.3 Hz, 8H), 0.87 (dt, J = 9.8, 6.9 Hz, 6H). ^{13}C NMR (151 MHz, acetone-d_6) δ 191.70, 150.41, 150.37, 149.47, 145.53, 144.29, 135.43, 130.24, 128.99, 124.13, 115.65, 115.43, 69.16, 69.11, 31.29, 31.28, 25.63, 25.62, 22.35, 13.38. MALDI-OF MS, experiment molecular weight is 458.62; the corresponding calculated value is 459.28.

Synthesis of 2. A mixture of 300 mg (416.6 mmol) of C_{60}, 200 mg (435.7 mmol) of 2′,5′-bis(hexyloxy)-4′-(pyridin-4-yl) biphenyl-4-carbalde-hyde and excess *N*-pyridylglycine were heated at reflux in 25 mL of chlorobenzene under argon for 6 h. The solution was washed with water and dried over magnesium sulfate. The solvent was removed by reduced pressure. The crude product was purified by flash column chromatography (eluent: CS_2/ethyl acetate = 1/12(v/v)), affording 370 mg (74%) of product **2**. ^{1}H NMR (600 MHz, $CDCl_3$) δ 8.63 (d, J = 4.0 Hz, 2H), 7.86 (s, 2H), 7.62 (dd, J = 38.1, 6.3 Hz, 4H), 7.02 (s, 1H), 6.96 (s, 1H), 5.01 (d, J = 11.8 Hz, 2H), 4.30 (d, J = 9.3 Hz, 1H), 3.96 (t, J = 6.4 Hz, 2H), 3.81 (t, J = 6.4 Hz, 2H), 2.87 (s, 3H), 1.69 (dd, J = 14.4, 6.8 Hz, 2H), 1.55 (dd, J = 14.1, 6.8 Hz, 2H), 1.42–1.33 (m, 2H), 1.23 (ddd, J = 16.1, 13.3, 5.1 Hz, 10H), 0.85 (dt, J = 10.6, 7.0 Hz, 6H). ^{13}C NMR (151 MHz, $CDCl_3$) δ 156.26, 154.04, 153.44, 153.42, 150.55, 150.46, 148.85, 147.33, 147.31, 146.84, 146.64, 146.50, 146.34, 146.31, 146.25, 146.23, 146.15, 146.13, 145.97, 145.79, 145.63, 145.57, 145.55, 145.48, 145.42, 145.34, 145.31, 145.27, 145.25, 145.18, 144.76, 144.61, 144.44, 144.40, 143.19, 143.06, 142.73, 142.64, 142.62, 142.31, 142.29, 142.20, 142.19, 142.14, 142.11, 142.08, 141.98, 141.83, 141.74, 141.57, 140.27, 140.22, 139.94, 139.49, 138.13, 136.91, 136.60, 135.97, 135.80, 132.28, 127.27, 124.38, 115.89, 115.71, 83.47, 70.15, 69.71, 69.50, 69.09, 40.15, 31.70, 31.66, 29.49, 26.00, 25.91, 22.93, 22.83, 14.36, 14.21. MALDI-OF MS, experiment molecular weight is 1209.1; the corresponding calculated value is 1208.3.

Crystallography

Black single crystals of **2** suitable for single-crystal X-ray diffraction were prepared by slowly diffuse *n*-hexane into a CS_2 solution of **2** at 273 K for 3 weeks. Crystal data of **2** was collected with the use of synchrotron radiation ($\lambda = 1.0331$ Å) at Beamline 11.3.1 at the Advanced Light Source, Lawrence Berkeley National Laboratory. The data were reduced utilizing Bruker SAINT, and a multi-scan absorption correction was applied using SADABS. The structure was solved with the direct method and refinement with SHELXL-2014.[33]

Crystal data for **2**: black blocks, 0.103 × 0.094 × 0.047 mm, orthorhombic, space group $P2_1/n$, $a = 18.0059(11)$ Å, $b = 9.9966(6)$ Å, $c = 32.4734(19)$ Å, $V = 5746.0(6)$ Å^3, $F_w = 2496$, $\lambda = 1.0331$ Å, $Z = 4$, $D_{calc} = 1.396$ Mg m^{-3}, $\mu = 0.198$ mm^{-1}, $T = 100$ K; 53 824 reflections, 13 098 unique reflections; 8707 with $I > 2\sigma(I)$; $R_1 = 0.1361$ [$I > 2\ \sigma(I)$], w$R_2 = 0.3484$ (all data), GOF (on F_2) = 1.093. The maximum residual electron density is 0.743 e Å^{-3}. CCDC-1578717 contains the crystallographic data for **2**.

DFT calculations were conducted with Gaussian 09 package[34] using the B3LYP functional with the 6-31G(d) basis set[35] for C, H, O, N atoms.

Conclusions

In summary, a novel fullerene derivative **2** bearing a rigid conjugated pyridine moiety is designed and synthesized by facile two-step reaction. Importantly, the structure of **2** has unambiguously determined by single crystal X-ray crystallography, showing its pyrrole ring structure with [6,6]-closed addition pattern. UV-vis spectrum of **2** exhibits relative higher absorption intensity than that of C_{60} in the range of 280–535 nm. Electrochemical results of **2** indicate that the rigid substituent on fullerene cage considerably raise LUMO energy level of **2** compared to that of C_{60}. Later, self-assembly of **2** by LLIP method with toluene as good solvent and hexane as poor solvent, afford two different microstructures with flower-like and discoid morphologies. Crystal packing of **2** unveils that the formation of flowerlike microstructure undergoes intermolecular dimers, ordered subunits processes consistent with proposed mechanism for self-assembly. The photocurrent response of these two morphologies was evaluated by photoelectrochemical cell measurement, demonstrating that flower-like microstructure has a higher value for photocurrent intensity than corresponding discoid microstructure due to facilitated charge carrier transport among them. The synergistic effect of synthesis strategy as well as self-assembly is beneficial to promote the applications of fullerene derivative in optoelectronic fields.

Conflicts of interest

There are no conflicts to declare.

Acknowledgements

We cordially thank Prof. Xing Lu, Dr Shushu Zheng for helpful discussion and advisory, and Dr Lipiao Bao for his kind help with single crystal structure analysis. This project was supported by the National Natural Science Foundation of China (NSFC, 51602097), Hubei Province Natural Science Foundation, China (2016CFB202) and Educational Commission of Hubei Province of China (No. Q20183002).

Notes and references

1 P. Brown and P. V. Kamat, *J. Am. Chem. Soc.*, 2008, **130**, 8890–8891.
2 H. Li, B. C. K. Tee, J. J. Cha, Y. Cui, J. W. Chung, S. Y. Lee and Z. Bao, *J. Am. Chem. Soc.*, 2012, **134**, 2760–2765.
3 C. Park, E. Yoon, M. Kawano, T. Joo and H. C. Choi, *Angew. Chem., Int. Ed.*, 2010, **49**, 9670–9675.
4 A. Kira, T. Umeyama, Y. Matano, K. Yoshida, S. Isoda, J. K. Park, D. Kim and H. Imahori, *J. Am. Chem. Soc.*, 2009, **131**, 3198–3200.
5 H. S. Shin, S. M. Yoon, Q. Tang, B. Chon, T. Joo and H. C. Choi, *Angew. Chem., Int. Ed.*, 2008, **47**, 693–696.
6 J. L. Segura, N. Martin and D. M. Guldi, *Chem. Soc. Rev.*, 2015, **34**, 31–47.
7 R. Bhosale, J. Misek, N. Sakai and S. Matile, *Chem. Soc. Rev.*, 2010, **39**, 138–149.
8 M. Sathish and K. Miyazawa, *J. Am. Chem. Soc.*, 2007, **129**, 13816–13817.
9 L. Wei, J. Yao and H. Fu, *ACS Nano*, 2013, **7**, 7573–7582.
10 S. S. Zheng, N. T. Cuong, S. Okada, T. Xu, W. Q. Shen, X. Lu and K. Tsukagoshi, *Chem. Mater.*, 2018, **30**, 7146–7153.
11 H. Liu, Y. Li, L. Jiang, H. Luo, S. Xiao, H. Fang, H. Li, D. Zhu, D. Yu, J. Xu and B. Xiang, *J. Am. Chem. Soc.*, 2002, **124**, 13370–13371.
12 C. Park, H. J. Song and H. C. Choi, *Chem. Commun.*, 2009, 4803–4805.
13 J. Geng, W. Zhou, P. Skelton, W. Yue, I. A. Kinloch, A. H. Windle and B. F. Johnson, *J. Am. Chem. Soc.*, 2018, **130**, 2527–2534.
14 X. Zhang and M. Takeuchi, *Angew. Chem., Int. Ed.*, 2009, **48**, 9646–9651.
15 A. M. Cassell, C. L. Asplund and J. M. Tour, *Angew. Chem., Int. Ed.*, 1999, **38**, 2403–2405.
16 J. F. Geng, W. Z. Zhou, P. Skelton, W. B. Yue, I. A. Kinloch, A. H. Windle and B. F. G. Johnson, *J. Am. Chem. Soc.*, 2008, **130**, 2527–2534.
17 M. Sathish, K. Miyazawa, J. P. Hill and K. Ariga, *J. Am. Chem. Soc.*, 2009, **131**, 6372–6373.
18 T. Homma, K. Harano, H. Isobe and E. Nakamura, *Angew. Chem., Int. Ed.*, 2010, **49**, 1665–1668.
19 T. Nakanishi, K. Ariga, T. Michinobu, K. Yoshida, H. Takahashi, T. Teranishi, H. MÖhwald and D. G. Kurth, *Small*, 2007, **3**, 2019–2023.
20 T. Nakanishi, Y. F. Shen, J. B. Wang, H. G. Li, P. Fernandes, K. Yoshida, S. Yagai, M. Takeuchi, K. Ariga, D. G. Kurth and H. Möhwald, *J. Mater. Chem.*, 2010, **20**, 1253–1260.
21 H. Asanuma, H. Li, T. Nakanishi and H. Mohwald, *Chemistry*, 2010, **16**, 9330–9338.
22 Y. F. Shen, A. G. Skirtach, T. Seki, S. Yagai, H. G. Li, H. Mohwald and T. Nakanishi, *J. Am. Chem. Soc.*, 2010, **132**, 8566–8568.

23 X. Zhang, T. Nakanishi, T. Ogawa, A. Saeki, S. Seki, Y. Shen, Y. Yamauchi and M. Takeuchi, *Chem. Commun.*, 2010, **46**, 8752–8754.
24 S. S. Babu, H. Mohwald and T. Nakanishi, *Chem. Soc. Rev.*, 2010, **39**, 4021–4035.
25 K. S. Kumar and A. Patnaik, *Langmuir*, 2011, **27**, 11017–11025.
26 A. Mitrović, N. Todorović, A. Žekić, D. Stanković, D. Milić and V. Maslak, *Eur. J. Org. Chem.*, 2013, **2013**, 2188–2193.
27 X. Zhang, X. D. Li, L. X. Ma and B. Zhang, *RSC Adv.*, 2014, **4**, 60342–60348.
28 H. Li, J. Choi and T. Nakanishi, *Langmuir*, 2013, **29**, 5394–5406.
29 K. S. Kumar and A. Patnaik, *Chemistry*, 2011, **17**, 5327–5343.
30 S. S. Zheng and X. Lu, *RSC Adv.*, 2015, **5**, 38202–38208.
31 Y. Xu, J. Guo, T. Wei, X. Chen, Q. Yang and S. F. Yang, *Nanoscale*, 2013, **5**, 1993–2001.
32 S. F. Yang, X. G. Wen, W. X. Zhang and S. H. Yang, *J. Electrochem. Soc.*, 2005, **152**, G220–G226.
33 G. M. Sheldrick, *Acta Crystallogr., Sect. C: Struct. Chem.*, 2015, **71**, 3–8.
34 M. J. Frisch, G. W. Trucks, H. B. Schlegel, G. E. Scuseria, M. A. Robb, J. R. Cheeseman, *et al.*, *Gaussian 09*, Gaussian, Inc., Wallingford CT, 2009.
35 W. J. Hehre, R. Ditchfield and J. A. Pople, *J. Chem. Phys.*, 1972, **56**, 2257–2261.